Amorphous HgCdTe infrared photoconductive detector with high detectivity above 200 K

Jun Wang,[1,2] Xiaoshuang Chen,[2,a)] Weida Hu,[2,b)] Lin Wang,[2] Wei Lu,[2] Faqiang Xu,[1] Jun Zhao,[3] Yanli Shi,[3] and Rongbin Ji[3]
[1]*National Synchrotron Radiation Laboratory, University of Science and Technology of China, Hefei, Anhui 230029, China*
[2]*National Laboratory for Infrared Physics, Shanghai Institute of Technical Physics, Chinese Academy of Sciences, Shanghai 200083, China*
[3]*Kunming Institute of Physics, Kunming, Yunnan 650223, China*

(Received 18 April 2011; accepted 18 August 2011; published online 13 September 2011)

Temperature dependence of dark current (I_d) and photocurrent (I_{ph}) is reported for Si-based amorphous HgCdTe (a-MCT) infrared photoconductive detector at 80-300 K. It is indicated that an uncooled a-MCT infrared detector can be fabricated based on the Si-based a-MCT. To describe the transport process, the Mott and Davis model [Davis and Mott, Philos. Mag. **22**, 903 (1970)] is proposed as the conducting model originally developed for amorphous silicon. A possible mechanism of the carrier transports is shown in the a-MCT materials. The transport transition between the localized and extended carriers leads to the maximal I_{ph}/I_d above 200 K. © *2011 American Institute of Physics*. [doi:10.1063/1.3638459]

Mercury cadmium telluride (MCT) is the most ideal and variable-gap material for the fabrication of infrared detectors.[1,2] However, the thermal expansion mismatch between the Si readout chip and the MCT-based infrared focal plane arrays (IRFPAs) constrains the format of IRFPAs.[3] The possible solution of the problem is that the silicon-based IRFPAs can satisfy the matching of the thermal expansion of the Si readout chip.[4] Thus, the use of Si substrate is very attractive in IRFPAs technology, not only because it is available in large area wafers but also the integration of the Si substrate with the Si readout integrated circuits (ROICs) allows fabrication of very large arrays. Consequently, the growth of MCT material on Si surface is desirable for the application of infrared detection. It is well known that As passivation of Si substrate has been the crucial step for the direct growth of single domain CdTe(211)B films on the Si(211) substrates.[5] Fortunately, by molecular beam epitaxy[6–8] and metalorganic vapor phase epitaxy[9–11] techniques, large-area high-quality CdTe(211)B layers have been grown on the As-passivated Si(211) surface for subsequent growth of MCT films. Additionally, the imaging of the Si-based infrared photodetector has been acquired.[8,12,13] As a variational way, one thinks easily whether a-MCT can be grown on the Si substrate. Some amorphous semiconductors, such as a-Si and a-C, have been already utilized in photovoltaic applications for the reasons of high conversion efficiency and low cost.[14–16] To realize the Si-based amorphous infrared photodetector, a-MCT growth on Si substrate is investigated.

In this letter, we report experimental and theoretical studies on the temperature dependence of I_d and I_{ph} for a-MCT infrared photoconductive detector. Meanwhile, the dynamic picture of carriers transport is discussed in detail.

The material used for device fabrication is a-MCT films grown on bottom electrode by RF magnetron sputtering technology. The Cadium composition of the a-MCT film is $x = 0.67$. The amorphous characteristic of the film is confirmed by the halo pattern of electron diffraction pattern as shown in Fig. 1(a), and the atomic force microscopy (AFM) surface morphology of a-MCT film is shown in Fig. 1(b). The detailed structure of device is shown in Fig. 1(c). I_{ph} is obtained by subtracting I_d from the measured photocurrent with the irradiation of infrared light 1.1 μm, and the power of the illumination source was 0.58 mW cm^{-2}. The performance of the device can be determined by the detectivity D^*.[17] As shown in Fig. 2(a), the a-MCT photoconductive device gets its maximal D^* above 200 K. In order to clarify the mechanism of characteristics of high operating temperature, I_d and I_{ph} are analyzed in detail. As shown in Figs. 3(a) and 3(b), I_d and I_{ph} are measured at different temperatures. Fig. 3(c) shows the I_{ph}/I_d of both the experimental and theoretical data with different temperatures.

Next, our main motivation is to explain the maximal I_{ph}/I_d at 210 K. According to Davis and Mott model,[18,19] a possible mechanism of the carrier transports is proposed for the a-MCT materials.

As shown in Fig. 3(a), I_{ph} increases with rising temperature markedly. In order to get an increasing result of I_{ph} with temperature, the localized potential barriers in extended states must be assumed. Fig. 4 illustrates the transport mechanism of a-MCT materials. The electrons get energy from the heat in the system and are carried into the extended states. But, due to the disordered effect, the localized potential barriers block the electronic transport. The electrons can cross the barriers by two methods: the thermally activated transport of electrons over the potential barriers and the quantum tunneling of electrons through the barriers. The process is similar to the carrier's transport through the crystalline grain boundary.[20–22]

The localized potential barriers E_b limit the carrier's transport in the conduction band. Consequently, the mobility is generally given by thermally emission over these barriers[20,23]

a)Electronic mail: xschen@mail.sitp.ac.cn.
b)Electronic mail: wdhu@mail.sitp.ac.cn.

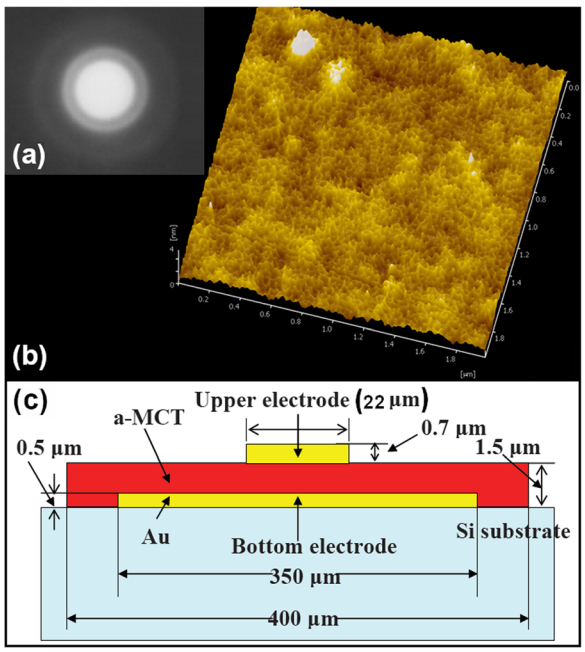

FIG. 1. (Color online) (a) Electron diffraction pattern and (b) AFM surface morphology of a-MCT film. (c) Schematic diagram of a-MCT infrared photoconductive detector structure.

$$\mu = \mu_0 + C\exp\left(-\frac{E_b}{k_B T}\right), \tag{1}$$

where C is a constant, k_B is the Boltzman constant, and T is the temperature. Assuming that the tunneling effect changes slowly with changing temperature, we can add the constant mobility factor μ_0 in the formula. Fig. 2(b) shows the drift mobility of a-MCT film at different temperatures. Here, we assume approximately that the drift mobility is equal the mobility of extended state. The dash line is the theoretical curve by fitting Eq. (1). The result indicates that the change of mobility with temperature is similar to the mobility change of the electrons by thermal emission transcending the potential barrier at grain boundary.[22]

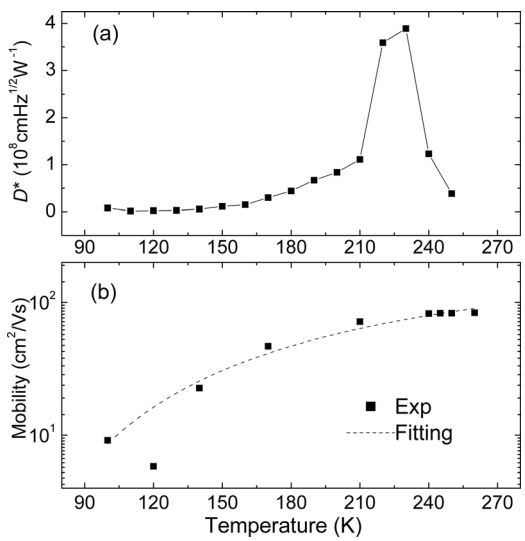

FIG. 2. (a) Temperature dependence detectivity with chopping frequency of 1000 Hz. (b) Drift mobility versus temperature for experiment (closed square) and theoretical result (dash line by fitting Eq. (1)).

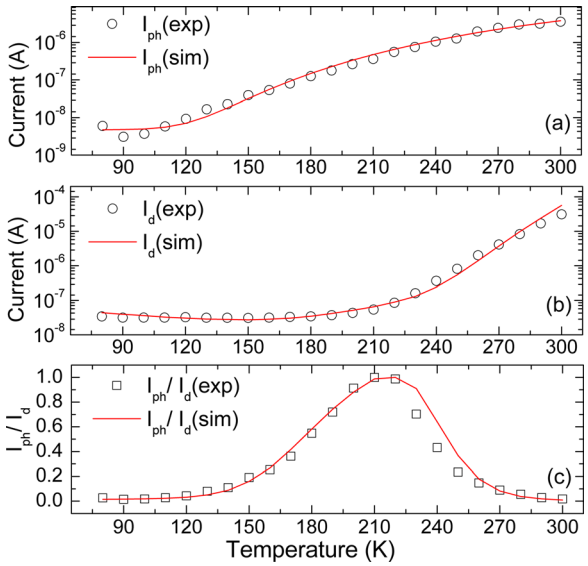

FIG. 3. (Color online) Comparisons of the experimental and calculated currents vs temperature at bias of 9.0 V. (a) I_{ph} and (b) I_d with the hollow circles and solid lines being the experimental and calculated results, respectively. The I_{ph}/I_d at different temperature is shown in (c). The hollow squares represent the measured values, and the solid line is the results of numerical calculations.

The density of electrons in an n-type semiconductor is given by[24]

$$n = \frac{1}{2}[N_D + (N_D^2 + 4n_i^2)^{\frac{1}{2}}], \tag{2}$$

where n_i is the intrinsic carriers density and N_D is the effective donor concentration. The density of electrons above the mobility edge E_C from the intrinsic excitation is[25]

$$n_i = \int_{E_C}^{\infty} N(E)\exp\left(-\frac{E - E_F}{k_B T}\right)dE. \tag{3}$$

Usually one can safely assume that the distribution N(E) of the density of states above the mobility edge does not change significantly on a $k_B T$ scale.[26] Hence, the intrinsic density of carriers can be written as

$$n_i = N(E_C)k_B T\exp\left(-\frac{E_C - E_F}{k_B T}\right) = AT\exp\left(-\frac{E_g}{k_B T}\right), \tag{4}$$

where A is a constant and $E_g \approx 1.0$ eV is the mobility gap.

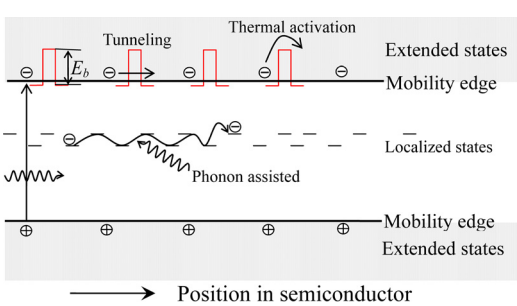

FIG. 4. (Color online) Electric conduction mechanisms are illustrated schematically for the electrons. Similar processes are also suitable for the holes.

Carriers can also transport in the band tails below the mobility edge, as shown in Fig. 4. The mobility can have the form[25]

$$\mu_{hop} = \frac{q v_{ph} R^2}{6kT} e^{-W/k_B T}, \quad (5)$$

where v_{ph} is the average phonon vibration frequency of the materials, q is the electron charge, R is the hopping distance in an average hopping range, and W is the obtained energy for the average hopping. For a typical phonon frequency $v_{ph} = 10^{13}\ s^{-1}$ and $W \approx k_B T$, Eq. (5) yields a mobility of the order $10^{-2}\ cm^{-2}\ V^{-1}$ at room temperature.[25] The mobility decreases roughly inversely with temperature and gives a relation of $\mu_{hop} \approx 3.0/T\ (cm^{-2}\ V^{-1})$.

The solid lines in Fig. 3 represent the *I-T* curves calculated by taking $\mu_0 = 0.02\ cm^{-2}\ V^{-1}$, $C = 2500\ cm^{-2}\ V^{-1}$, $E_b = 0.13$ eV, and $A = 5 \times 10^{18}\ cm^{-3}\ K^{-1}$. For our sample, in the temperature range of 80–210 K, the main electric conduction of I_d is from the localized states below the mobility edge. The mobility decreases roughly inversely with temperature as described in Eq. (5). However, I_{ph} is mainly derived from the carriers of the extended states, and the mobility increases with increasing temperature by Eq. (1). Thus, I_{ph}/I_d increases gradually with increasing temperature in the range of 80–210 K.

As the temperature increases, more and more electrons are thermally excited into the extended states. The carrier's conduction of localized states, contributed to dominant I_d, changes into that of extended states. I_d is determined by both the mobility and electron density of the extended state. It is also known that the mobility and electron density increased with temperature increasing. Finally, the increasing rate of I_{ph} is slower than that of I_d although the mobility also rises as temperature increases. Therefore, the ratio of I_{ph}/I_d decreases with increasing temperature at the range of 210–300 K.

In summary, we have studied the temperature dependence of I_{ph} and I_d for Si-based a-MCT infrared photoconductive detector. The dynamic picture of carriers transport is discussed in detail. It is thought that the maximum I_{ph}/I_d is caused by the conductive change between the localized and extended carriers. Such an interesting characteristic can be used to fabricate the uncooled Si-based a-MCT infrared detectors.

This work was supported in part by the State Key Program for Basic Research of China (2007CB613206, 2011CB922004), National Natural Science Foundation of China (10725418, 10734090, 10990104, 60976092, 10874196, and 61006090), Key Fund of Shanghai Science and Technology Foundation (09DJ1400203, 09dz2202200, 10JC1416100, and 10510704700), Knowledge Innovation Program of the Chinese Academy of Sciences and the computational support from Shanghai Supercomputer Center.

[1] A. Rogalski, Prog. Quantum Electron. **27**, 59 (2004).
[2] A. Rogalski, J. Antoszewski, and L. Faraone, J. Appl. Phys. **105**, 091101 (2009).
[3] Y. Huang, X. S. Chen, H. Duan, and W. Lu, J. Electron. Mater. **36**, 925 (2007).
[4] A. Rogalski, Rep. Prog. Phys. **68**, 2267 (2005).
[5] N. K. Dhar, P. R. Boyd, M. Martinka, J. H. Dinan, L. A. Almeida, and N. Goldsman, J. Electron. Mater. **32**, 717 (2003).
[6] J. B. Varesi, A. A. Buell, J. M. Peterson, R. E. Bornfreund, M. F. Vilela, W. A. Radford, and S. M. Johnson, J. Electron. Mater. **32**, 661 (2003).
[7] S. Rujirawat, L. A. Almeida, Y. P. Chen, S. Sivananthan, and D. J. Smith, Appl. Phys. Lett. **71**, 1810 (1997).
[8] J. B. Varesi, R. E. Bornfreund, A. C. Childs, W. A. Radford, K. D. Maranowski, J. M. Peterson, S. M. Johnson, L. M. Giegerich, T. J. de Lyon, and J. E. Jensen, J. Electron. Mater. **30**, 566 (2001).
[9] M. Niraula, K. Yasuda, H. Ohnishi, H. Takahashi, K. Eguchi, K. Noda, and Y. Agata, J. Electron. Mater. **35**, 1257 (2006).
[10] K. Shigenaka, K. Matsushita, L. Sugiura, F. Nakata, and K. Hirahara, J. Electron. Mater. **25**, 1347 (1996).
[11] H. Ebe, T. Okamoto, H. Nishio, T. Saito, Y. Nishijima, M. Uchikoshi, M. Nagashima, and H. Wada, J. Electron. Mater. **25**, 1358 (1996).
[12] J. M. Peterson, J. A. Franklin, M. Readdy, S. M. Johnson, E. Smith, W. A. Radford, and I. Kasai, J. Electron. Mater. **35**, 1283 (2006).
[13] R. Bornfreund, J. P. Rosbeck, Y. N. Thai, E. P. Smith, D. D. Lofgreen, M. F. Vilela, A. A. Buell, M. D. Newton, K. Kosai, S. M. Johnson, T. J. Delyon, J. J. Jensen, and M. Z. Tidrow, J. Electron. Mater. **36**, 1085 (2007).
[14] J. C. Kong, S. L. Wang, L. D. Kong, J. Zhao, Y. Ma, G. H. Wang, X. J. Li, L. L. Yang, P. J. Zhang, and R. B. Ji, Proc. SPIE **7383**, 73833Y (2009).
[15] E. Maruyama, S. Okamoto, A. Terakawa, W. Shinohara, M. Tanaka, and S. Kiyama, Sol. Energy. Mater. Sol. Cell **74**, 339 (2002).
[16] H. A. Yu, Y. Kaneko, S. Yoshimura, and S. Otani, Appl. Phys. Lett. **68**, 547 (1996).
[17] R. M. Broundy and V. J. Mazurczyck, *Semiconductors and Semimetals*, edited by R. K. Willarason and A. C. Beer (Academic, New York, 1981), Vol. 18, Chap. 5, p. 159.
[18] E. A. Davis and N. F. Mott, Philos. Mag. **22**, 903 (1970).
[19] N. F. Mott and E. A. Davis, *Electronic Processes in Non-Crystalline Materials* (New York, Oxford University Press, 1971).
[20] J. Y. W. Seto, J. Appl. Phys. **46**, 5247 (1975).
[21] G. Baccarani, B. Ricco, and G. Spadini, J. Appl. Phys. **49**, 5565 (1978).
[22] J. H. Schon and C. Kloc, Appl. Phys. Lett. **78**, 3821 (2001).
[23] J. W. Orton and M. J. Powell, Rep. Prog. Phys. **43**, 1263 (1980).
[24] S. M. Sze and K. K. Ng, *Physics of Semiconductor Devices*, 3rd ed. (Wiley, Hoboken, New Jersey, 2007), p. 25.
[25] P. Nagles, *Amorphous Semiconductors in Topics in Applied physics* (Springer, Berlin, 1979), Vol. 36, Chap. 5.
[26] H. Overhof and P. Thomas, *Electronic Transport in Hydrogenated Amorphous Semiconductors in Springer Tracts in Modern Physics* (Springer, Berlin, 1989), Vol. 114, p. 24.